Engineering Structures 220 (2020) 110867

Contents lists available at ScienceDirect

Engineering Structures

journal homepage: www.elsevier.com/locate/engstruct

Dynamic shear amplification of reinforced concrete coupled walls

Leonardo M. Massone[a,*], Enrique Bass[b]

[a] Department of Civil Engineering, University of Chile, Blanco Encalada 2002, Santiago, Chile
[b] University of Chile, Chile

ARTICLE INFO

Keywords:
Shear amplification
Dynamic
Shearwall
Model
Coupling

ABSTRACT

Dynamic shear amplification has been commonly studied in cantilever reinforced concrete wall systems, however, coupling beams or slabs can generate axial loads that can modify the response. A parametric study is carried out that covers 432 nonlinear time-history analyses (72 models with 6 records) of 2 coupled walls with different length, including variations in the amount of boundary element steel ratio (1%, 3% and 5%), amount of slab steel ratio (0.0%, 0.3% and 0.6% − 0.0% is defined for connected walls without coupling), building height (25 m, 50 m and 75 m), and wall length (2 m, 4 m and 6 m). The walls are represented with nonlinear fiber models; while the coupling slabs are elastic within the length with a rigid-perfectly plastic model at both element ends. The shear amplification values depend on the coupling level, with the highest amplification values being observed for connected (not coupled) systems. The high values for connected walls are due to the rapid plastification of the wall because of the low structural redundancy. The mean shear amplification values are 1.45, 1.10 and 1.35 for coupling slabs with reinforcing steel ratio of 0.0%, 0.3% and 0.6%, respectively. The proposed expression for the dynamic shear amplification also depends on the response modification factor of the walls, a parameter directly related to nonlinearity sources. On the other hand, an expression used by many codes that depends on the number of floors does not necessarily represent the amplification that occurs in tall buildings with moderate coupling, since the plastification at the base in such cases is difficult to achieve given their large elastic displacement capacity, as well as, cases that incorporate a minimum base shear criterion, that reduce the nonlinearity incursions.

1. Introduction

One of the most used tools for seismic design of buildings is the spectral modal analysis (SMA), which is a method that uses the linear properties of materials to estimate the response in terms of displacements and inertial forces that a structure is subjected for seismic design. The SMA method delivers the global response through resolving N systems of one degree of freedom, and internal loads are determined by a combination method. Broadly speaking, the advantage of the SMA is that it avoids carrying out a dynamic time-history analysis (THA), such that, it evaluates the modal response for a design spectrum, combining representative periods of the structure. On the other hand, the SMA has certain limitations, since it commonly considers that the response modification factor, required to determine the design forces, applies equally to all vibration modes, while nonlinearity is commonly concentrated in the fundamental mode. Moreover, the SMA as a linear-elastic analysis, it assumes a linear behavior of the structural elements, not allowing stiffness changes due to cracking or yielding, for example.

In the SMA, the distribution of inertial forces for the linear case is commonly close to an inverted triangular (fundamental mode) shape, such that the resulting height of inertial forces is located at $h_{ef} \approx 2/3h_w$ (h_w, height of the building). If the longitudinal reinforcement at the base of a cantilever wall has yielded (nonlinear) and the wall lateral force distribution at that instant resembles more or less an even distribution in height, as shown in Fig. 1, due to the plastification at the base (effect of higher modes), it yields that $h_{ef} \approx 1/2h_w$. The shear amplification (ω) for this case can be defined as the ratio between the base shear obtained from a conventional analysis (e.g., SMA) and the base shear from a nonlinear model (e.g., nonlinear time-history analysis or NLTHA), which in the case of identical base moment is equivalent to the ratio of the height of inertial forces, and would be approximately, $\omega = \frac{V_{b[SMA]}}{V_{b[NLTHA]}} = \frac{2/3h_w}{1/2h_w} \approx 1.33$. Larger participation of equivalent higher modes in the nonlinear analysis can lead to a resultant lateral force at an even lower level, yielding even larger shear amplification values. The general concept of dynamic shear amplification can be understood as the change in the distribution of inertial forces given the strength limitation and decrease in stiffness at the plastic hinge location (e.g., wall base). In the case of cantilever walls the only source of material

* Corresponding author.
E-mail address: lmassone@ing.uchile.cl (L.M. Massone).

https://doi.org/10.1016/j.engstruct.2020.110867
Received 10 October 2019; Received in revised form 13 May 2020; Accepted 26 May 2020
Available online 26 June 2020
0141-0296/

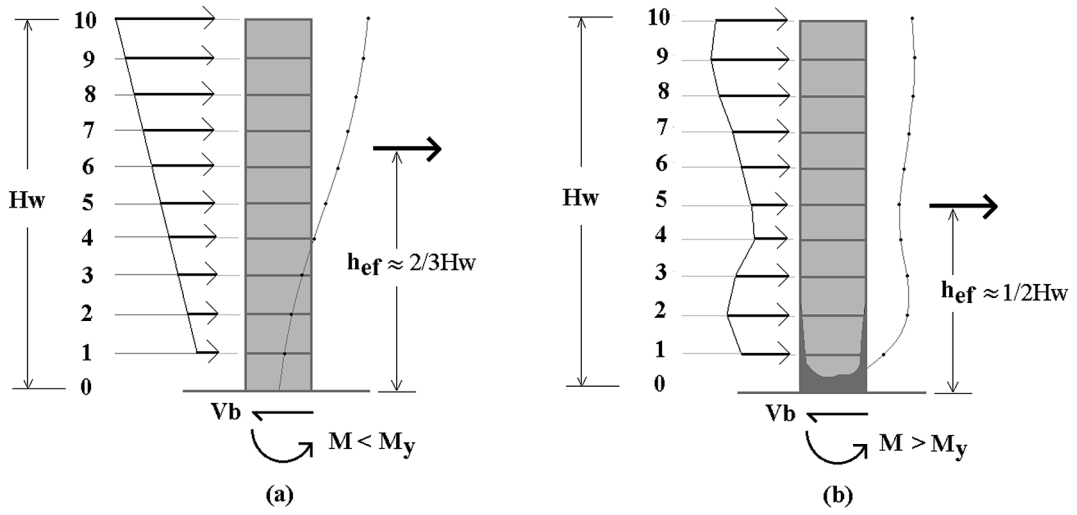

Fig. 1. (a) Distribution of inertial forces for the linear response – SMA, and (b) distribution of inertial forces for the nonlinear response – NLTH.

nonlinearity is the plastification of the base, such that, once yielding has occurred, the effects of amplification are imminent through the presence of higher modes.

The work by Blakeley et al. [1] for cantilever reinforced concrete walls demonstrated the relevance of the higher modes in the shear response once the wall reached yielding at the base. This study was conducted with three models of 6, 15 and 20-story buildings, for 5 acceleration records of which two were constructed artificially. Its results meant a change in the seismic-resistant design provisions of New Zealand in 1982, recognizing the dynamic amplification effects for the design of reinforced concrete walls and the European-International Concrete Committee (CEB) in its 1980 edition, and currently in ACI 318 in its 2019 version. Eq. (1) that describes the dynamic shear amplification factor (), dependent on the number of floors (n), is included in the NZS 3101 [2] and ACI 318 [3] codes.

$$\omega_v = \begin{cases} 0.9 + \frac{n}{10}, \text{if } n \le 6 \\ 1.3 + \frac{n}{30} \le 1.8, \text{if } n > 6 \end{cases} \quad (1)$$

Derecho et al. [4] developed a parametric study for 10 and 40-story buildings for 6 acceleration records using a nonlinear model of the walls under a time-history analysis. The results indicate that the dynamic shear amplification depends on the rotational ductility and the fundamental period of the structure, demonstrating that this behavior is highly influenced by the level of the nonlinear incursion. Similarly, Eibl and Kentzel [5] proposed an expression to quantify the dynamic shear amplification, where the formulation assumes that only the fundamental mode is limited by the wall plastification, maintaining linear response for the second mode, standing out the effect of nonlinear response associated to the first mode. This formulation was adopted by Eurocode 8 Part 1 [6]. Priestley [7] proposed a similar formulation, but for several modes.

Moreover, dynamic shear amplification has been observed in experimental tests as well. Panagiotou and Restrepo [8] observed a base moment over-strength, defined as the ratio of the maximum measured base moment and the design base moment, of 2.7; while base shear over-strength factor was 4.2, noticing an increase of 50% for shear. Eberhard and Sozen [9] conducted small-scale dynamic tests with dual wall systems and 9 and 10-story moment frames on a shake table to observe the effect of shear amplification in reinforced concrete wall systems. In their investigation, they noted that as the system was damaged, the distribution of inertial forces behaved differently once yielding at the base was reached, generating significant increment in shear forces in the elements.

Although the dynamic shear amplification phenomenon has been known for several years, most design formulations are based on analytical developments for cantilever walls. The little information on coupled walls is usually associated with limited case studies, for symmetrical walls and considering beams as coupling elements that usually cause large variations of axial loads on walls (e.g., [10]). However, it is common to observe coupled walls or a series of walls with different dimensions coupled through beams or slabs in Chile and other places such as Europe and Japan. For this reason, this work addresses the effect of coupling on shear amplification through a series of nonlinear dynamic analysis for non-symmetric coupled walls.

2. Formulation of amplification in coupled walls

Let us consider the case of two walls with the same geometric properties and coupled with reinforced concrete slabs (Fig. 2). If a time-history linear response analysis is performed, and only earthquake actions are considered, similar values are obtained for shear and moment

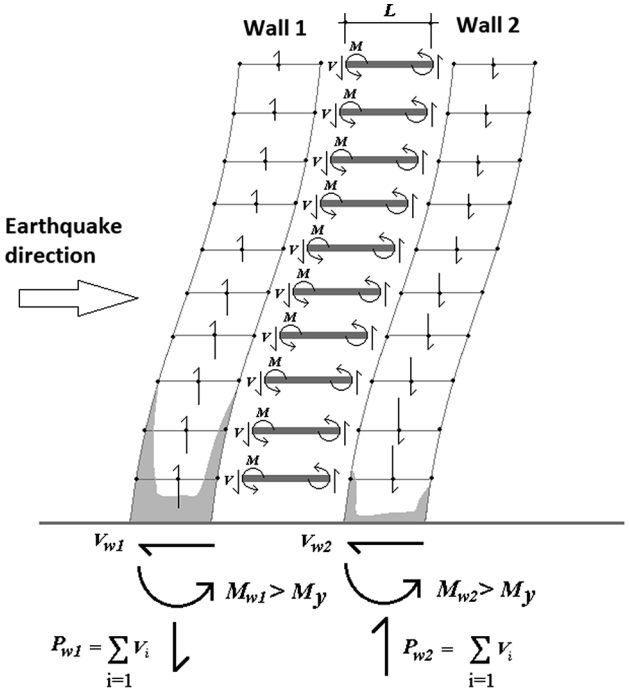

Fig. 2. Effect of the coupling wall system.

distribution in each of the walls. However, the coupling elements have shear forces at both ends that increase the axial load of one wall and decrease the axial load of the other wall. On the other hand, when accounting for the nonlinear response, the flexural strength of an element depends on the level of axial load, indicating that the shear and moment distribution cannot be similar if the flexural strength is different for both walls. Fig. 2 shows the wall response at a time in which the coupling elements have yielded from the first to the last floor. By this time, wall 1 has a much lower axial load level than wall 2. This decrease in axial load on wall 1 causes a lower moment capacity. Such an effect might change for large axial gravity loads. The increase (or decrease) in the flexural strength of an element under axial loads is decisive in the distribution of shear forces and moment in the system, creating migration of forces to the stronger wall. In the case of coupled walls with different lengths, the response also requires understanding the impact of such variable since a cantilever larger wall would yield at a smaller lateral drift displacement than a narrower wall, since yield displacement ($\delta_y \propto \phi_y h_w^2$, where h_w is the height of the wall) is proportional to the yield curvature ($\phi_y \propto \frac{\varepsilon_y}{l_w}$), and yield curvature is proportional to the yield strain (ε_y) and inversely proportional to the wall length (l_w). Therefore, a reduction of axial load might not be decisive. Thus, a parametric study is carried out to understand the behavior of coupled walls with different lengths.

2.1. General description of the model

The model of the structural system is created with frame elements (equivalent beam-column model) commonly used for slender walls where the connection of walls with coupling elements is achieved with infinitely rigid elements. The two-dimensional model has its base fixed.

Fig. 3a shows a general scheme of a section that includes one coupling element and portions of the two walls connected. For the walls, each story is divided into 5 elements (0.5 m height each) using a concentrated plasticity model defined by a fiber section that employs uniaxial stress-strain models for unconfined concrete for the wall web, confined concrete for the confined boundary elements and steel for the longitudinal reinforcement [11]. For the coupling elements (reinforced concrete slabs in this case, although results can be extended to beams with the same flexural strength), the nonlinearity is defined exclusively by their flexural behavior, modeled with concentrated plasticity with rigid-perfectly plastic behavior at the element ends with a plastic moment defined as the nominal flexural strength (M_n), maintaining a linear behavior for the rest of the element [12]. Thus, nonlinearity for coupling elements is only observed once M_n is reached allowing free-rotation afterward at element ends (maintaining the moment). This simple model can capture the moment strength of the slab, which causes the variation of axial load in walls. The walls are connected by a slab with a thickness of 20 cm, an effective width of 200 cm, and a clear span of 1.5 m (common aisle width) between walls (Fig. 3b). Fig. 3b shows a scheme of one story with the dimensions of the principal elements. The parametric analysis considers variations of the steel ratio of the boundary elements, the steel ratio of the coupling elements, the length of the longer wall (M1) and the number of stories.

The gravitational axial load level is directly related to the number of floors, so that for the 10, 20 and 30-story models an axial load level at the base of $0.075A_g f'_c$, $0.1A_g f'_c$ and $0.125A_g f'_c$ was selected, respectively [13]. The inertial mass was defined based on the gravity loads. Fig. 4 shows the two-dimensional models used in the study for the case of 10 floors, as an example. In all cases, a wall of 2 m and another variable of 2 m, 4 m and 6 m are considered to observe the effect of the coupling on symmetric and non-symmetric walls. The discretization of the cross-section depends on the length of the element, for $L_{w1} = 2$ m there are 33 fibers, for $L_{w1} = 4$ m there are 40 fibers and for $L_{w1} = 6$ m there are 46 fibers. Further discretization, such as doubling the number of elements or fibers, shows a little variation of results, with shear amplification differences less than 5% in most cases. It should be noted that, in the case of 30 floors, the cases in which both walls have the same length of 2 m ($L_{w1} = L_{w2} = 2$ m) were not considered, since they presented fundamental periods far from what was commonly observed in Chilean buildings [14]. The walls have a thickness of 30 cm for all cases [13]. A steel ratio of 1%, 3% or 5% was selected for the boundary elements for the variable walls (a steel ratio of 1% was selected for the wall of a constant length of 2 m), based on a depth of the boundary element of 15% of the wall length. For the vertical web reinforcement, a common value of 0.38% is found in Chilean wall construction [13], which is used in this work. For coupling elements, cross-sectional dimensions of 200 cm (width) by 20 cm (height) are used, together with a steel ratio of 0.0% (connected walls), 0.3% and 0.6% (coupled walls). The 0.0% of steel reinforcement in slabs defines a hinge at the slab ends, creating a uniaxial element between walls working in either tension or

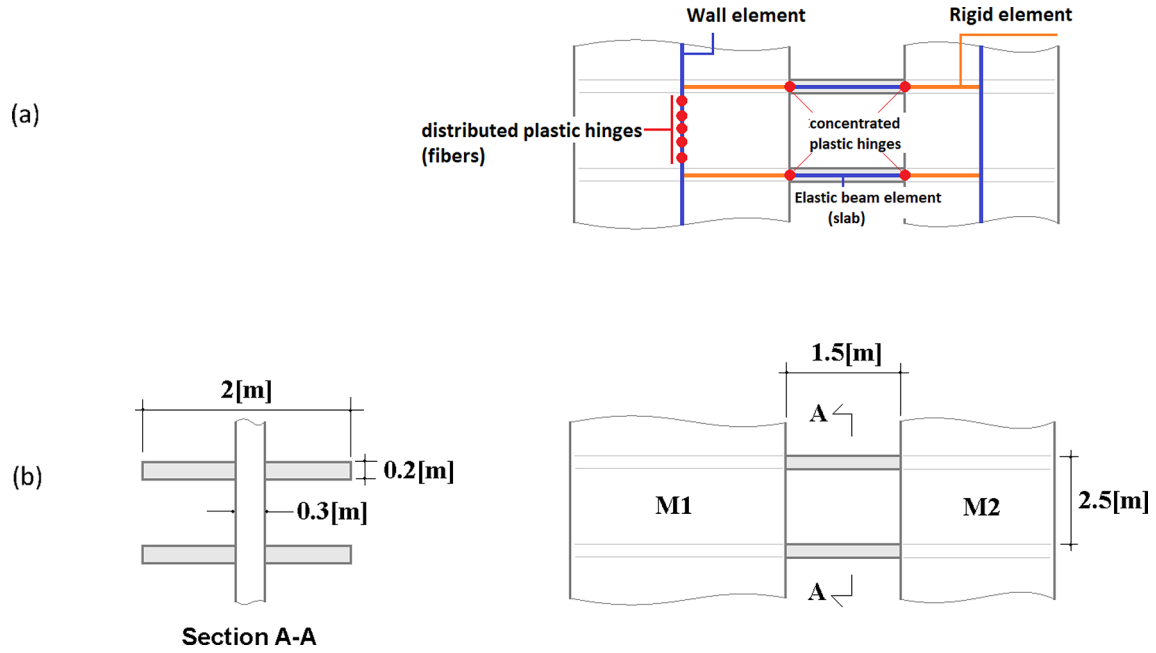

Fig. 3. (a) Beam-column equivalent model for the 2D parametric study, and (b) interstory wall and slab scheme.

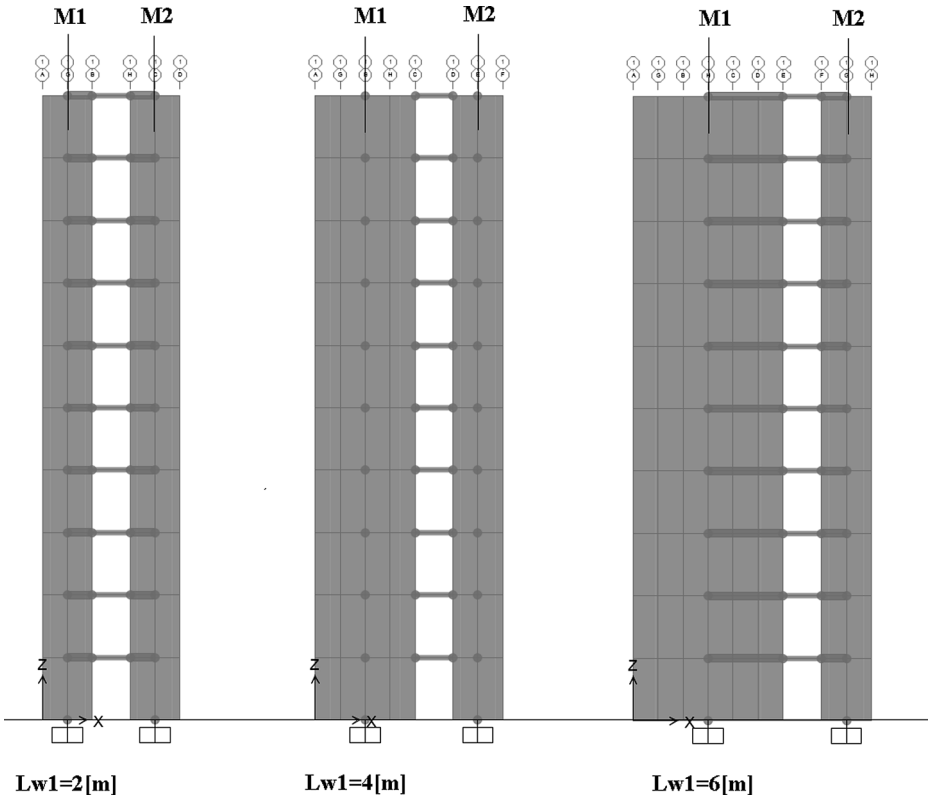

Fig. 4. Base model for 10-story buildings for variable wall length (M1) of - (a) 2 m, (b) 4 m, and (c) 6 m.

Table 1
Fundamental period and characteristics of models.

Fundamental Period (*T1*)			Characteristics		
10 stories	20 stories	30 stories	lw1	ρb	ρs
[s]	[s]	[s]	[m]	%	%
1.25	3.85	–	2	1	0.0
0.53	1.36	–	2	1	0.3
0.53	1.36	–	2	1	0.6
1.22	3.75	–	2	3	0.0
0.53	1.34	–	2	3	0.3
0.53	1.34	–	2	3	0.6
1.19	3.67	–	2	5	0.0
0.52	1.33	–	2	5	0.3
0.52	1.33	–	2	5	0.6
0.73	2.23	4.47	4	1	0.0
0.42	1.08	2.05	4	1	0.3
0.42	1.08	2.05	4	1	0.6
0.70	2.13	4.28	4	3	0.0
0.41	1.06	2.02	4	3	0.3
0.41	1.06	2.02	4	3	0.6
0.67	2.05	4.12	4	5	0.0
0.41	1.05	1.99	4	5	0.3
0.41	1.05	1.99	4	5	0.6
0.48	1.46	2.94	6	1	0.0
0.34	0.89	1.70	6	1	0.3
0.34	0.89	1.70	6	1	0.6
0.46	1.40	2.80	6	3	0.0
0.34	0.87	1.67	6	3	0.3
0.34	0.87	1.67	6	3	0.6
0.44	1.34	2.69	6	5	0.0
0.33	0.86	1.64	6	5	0.3
0.33	0.86	1.64	6	5	0.6

lw1 = length of wall 1.
ρb = boundary steel ratio.
ρs = slab steel ratio.

Table 2
PGA, Arias intensity and average frequency of records for analysis.

Location	Event	PGA[/g]	IA[m/s]	*fm*[Hz]
CONCEPCION CENTRO	Maule 2010	0.41	9.09	0.92
CONCEPCION SAN PEDRO	Maule 2010	0.61	14.75	4.61
CONSTITUCION	Maule 2010	0.65	27.22	2.01
LLOLLEO	Maule 2010	0.56	10.55	2.73
MATANZAS	Maule 2010	0.34	7.10	1.67
SAN ISIDRO	Valparaiso 1985	0.72	19.81	3.06

compression (called “connected”) that forces lateral displacement compatibility. Since the slab model considers only variations of the longitudinal reinforcement quantity, which varies the level of coupling that could be achieved in the slabs, in the text the term “coupling” is associated with the other two different levels of reinforcement in slabs. Considering the different length of walls Lw_1 (2 m, 4 m and 6 m), the numbers of floors (10, 20 and 30), the steel amount in boundary elements (1%, 3% and 5%) and the steel amount in coupling elements (0, 0.3% and 0.6%), the total number of analyses is 81 cases. However, considering that the 30-story building case does not include the wall length $Lw_1 = 2$ m, it reduces this to 72 cases (Table 1), which are analyzed with a series of six records (Table 2). The selection of records considered large records, among the few available, in terms of Arias Intensity with a variety of frequency content available in Chile for subduction earthquakes that are mostly consistent with the design spectrum.

Normal strength material properties are used for the analysis. For concrete, a compression strength of $f'_c = 25$ MPa is considered, whereas for steel the yield stress is $f_y = 420$ MPa. The wall web (zone other than the boundary elements) is characterized by unconfined concrete. For the construction of the stress-strain curve of unconfined concrete in compression, three zones are identified: first, a parabolic behavior until reaching the peak stress (f'_c) at a strain of 0.002; then a linear descent until a strain of 0.0038 for a strength reduction of 15%; and finally, a

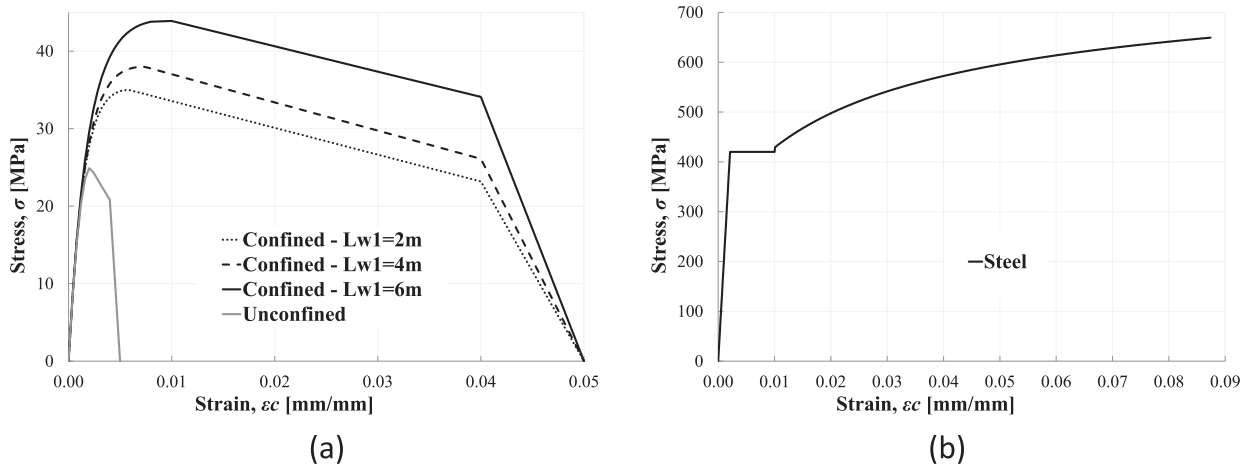

Fig. 5. Material constitutive laws - (a) concrete in compression, and (b) steel.

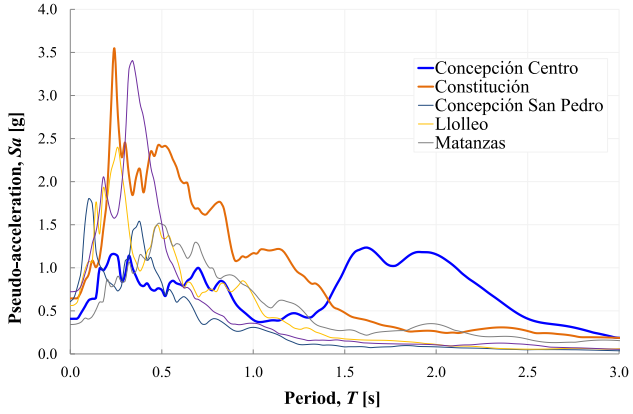

Fig. 6. Pseudo-acceleration spectrum for seismic records.

linear descent to zero strength at a strain of 0.005 (Fig. 5a). On the other hand, for tension, the strength is set as 3.1 MPa at a strain of 0.00013 to capture cracking in walls. The boundary wall elements are characterized by confined concrete. The work by Saatcioglu and Razvi [15] is used for the construction of the stress–strain curve of confined concrete. Considering a wall boundary detailing consistent with ACI 318–19 for a transversal steel ratio close to 1% in both directions, the compression strength of concrete increases to 35 MPa, 38 MPa and 44 MPa for wall lengths of 2 m, 4 m and 6 m, respectively (Fig. 5a). The level of confinement of wall boundary elements was enough to guarantee a stable response without strength degradation [16]. For the construction of the stress-strain curve of the reinforcing steel three zones are identified: first, a linear behavior until reaching the yield strain of $\varepsilon_y = 0.0021$; then a yield plateau until a strain of $\varepsilon_{sh} = 0.01$ is reached; and finally, the hardening zone reaching a maximum stress of 650 MPa for a strain of $\varepsilon_u = 0.09$ (Fig. 5b).

2.2. Time-history analysis

Two nonlinear time-history analyses are carried out in SAP2000 [17] to determine the dynamic shear amplification for coupled walls. The first one seeks to capture the linear properties of the system, so that the acceleration in the analysis is reduced by a factor of 100 (equivalent linear history time analysis) avoiding even cracking of concrete, but then scaled up back again for comparison (e.g., base moment). The second uses actual acceleration records to obtain the nonlinear response of the system. A classic Rayleigh damping matrix is used, with a damping ratio of 5%, which is commonly defined for reinforced concrete structures in most seismic design standards and has been used in previous similar studies. Other damping values would cause variability in the inelastic incursion, which can be evaluated with the ratio between the linear moment and the nonlinear moment of the wall. Table 1 shows the fundamental periods of the two-dimensional models used in the study. It can be seen that the range of periods goes from 0.33 s to 2.05 s for buildings with coupling, yielding an H/T (building height/period) value between 37 m/s and 76 m/s for all cases with coupling, which is consistent with a range of periods observed in buildings commonly found in Chile [14].

To check the potential resonance of the selected records and the natural period of the models, the average frequency of a record is calculated according to the equation proposed by Rathje et al. [18] as $f_m = \frac{\sum_{i=1}^{n} C_i^2}{\sum_{i=1}^{n} C_i^2 / f_i}$, where C_i corresponds to the amplitudes and f_i to the frequencies of the fast Fourier transform.

Table 2 shows relevant characteristic values of ground records used in this study, such as average frequency, peak ground acceleration (PGA), and Arias intensity. The average frequencies of the records are within a range between 0.92 Hz and 4.61 Hz (0.22 s to 1.1 s), so that it is similar to the fundamental frequencies of the proposed models that fall within a range between 0.49 Hz and 3.05 Hz (0.33 s to 2.05 s). Fig. 6 shows the pseudo-acceleration response spectra of the records used in this study. It can be noted that the response spectra constructed from the acceleration records present spectral forms typically found in subduction earthquake records with a predominant period, however, pseudo-acceleration spectrum with a double peak is observed in the Conception Centro record, which can be expected to affect both rigid and flexible structures.

2.3. Validation of model formulation

To validate the formulation of the model, a dynamic test carried out on a scaled cantilever wall [19] and a cyclic quasi-static test of a slender wall with well-distributed damage [20] were considered for modeling comparison in this work.

In the case of the dynamic test, one specimen, from an experimental program carried out on RC rectangular scaled (1:10) walls and tested on a unidirectional shaking table (Fig. 7a), was considered. The wall is 4 cm thick, 2.15 m high and 15 cm long. For the test setup, several steel plates are disposed to add inertial and axial forces to the specimens during testing, resulting in a total axial force of $0.07 f'_c A_g$ for nominal concrete strength. Damage is concentrated at the wall base, primarily due to flexure with some participation of shear. For the Constitución 2010 record (Table 2, Fig. 6), an amplification of about 1.3 is obtained. A model consistent with the one proposed in this work estimated the peak roof displacement with an error of less than 10% in the positive and negative directions (Fig. 8a). In the case of the shear force, the

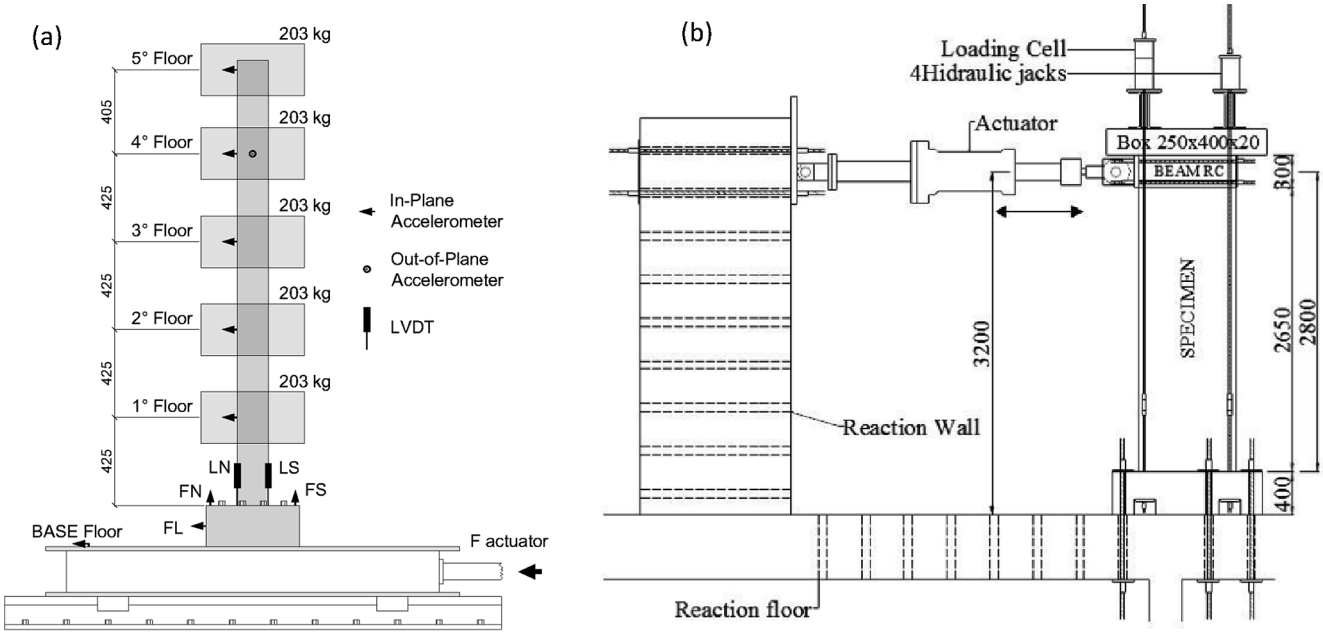

Fig. 7. Test setup of specimens for model validation – (a) dynamic test [19], and (b) quasi-static test [20].

prediction error reached an average value of approximately 10% between both directions (Fig. 8b), while in the case of the moment this value is approximately 5% (Fig. 8c).

In the case of the quasi-static wall test, one specimen from an experimental program on RC walls was considered. The specimen was tested under a nominal constant axial load of $0.1f'_cA_g$ and cyclic lateral loads with increasing drift levels. The specimen was 2.65 m tall, 15 cm thick, and 90 cm long (Fig. 7b). Similar to the dynamic case, the failure was located at the wall base, but in this case, detailing of the wall boundary element was based on ACI 318 [3] given the larger size of the

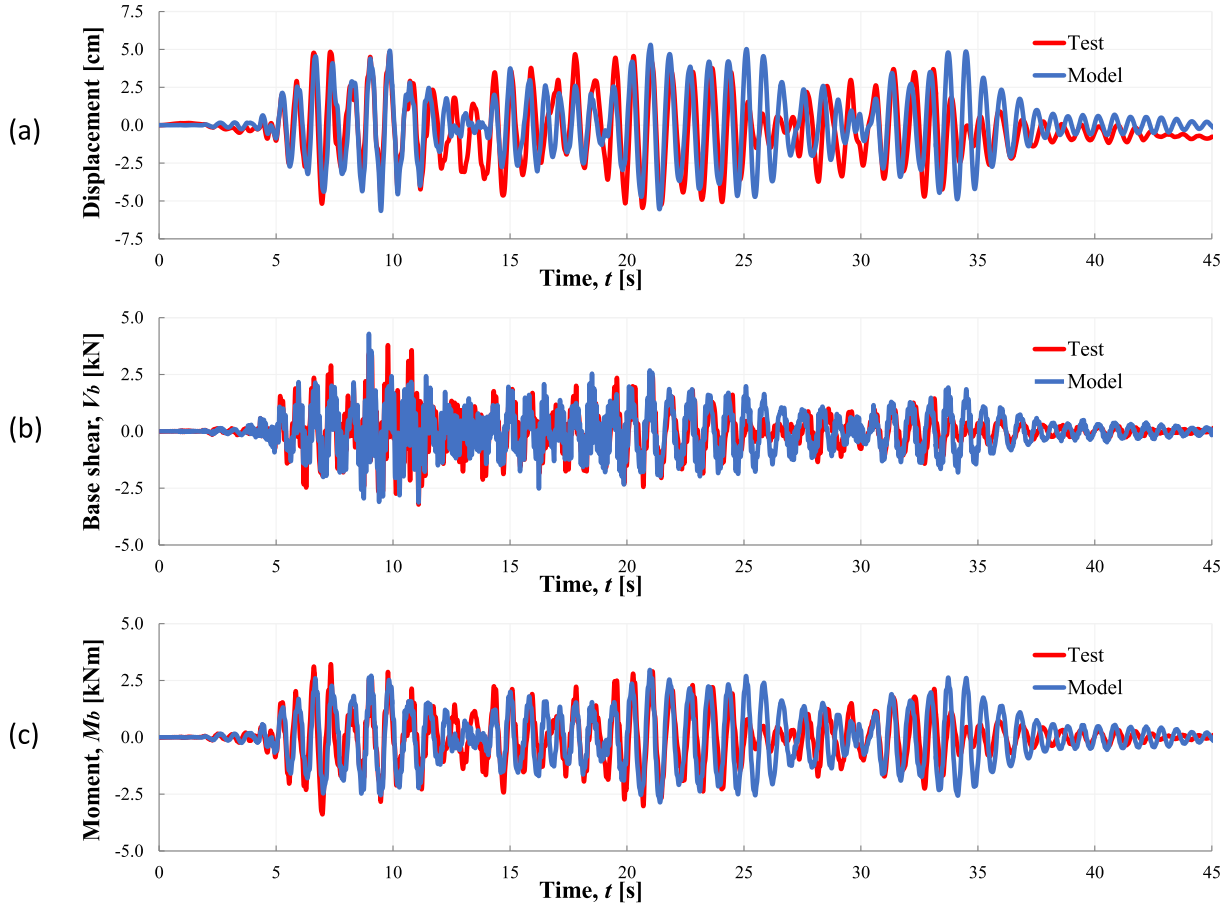

Fig. 8. Dynamic test result and model comparison – (a) top displacement, (b) base shear, and (c) base moment.

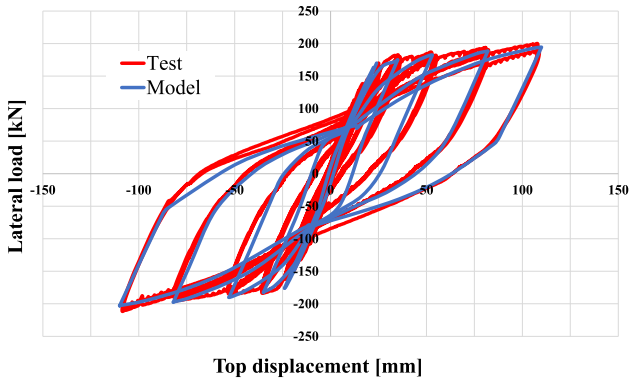

Fig. 9. Quasi-static test result and model comparison – lateral load versus top displacement.

specimen, reaching a large drift level. The overall load versus displacement response was obtained based on a model consistent with the formulation described in this work. The differences in the estimation of the maximum load per cycle after yielding are less than 10% in each cycle (Fig. 9).

According to the results, it can be considered that the model is appropriate for its use in this work. More details can be obtained elsewhere [21].

3. Analysis of results

The equivalent response modification factor, R_{eq}, represents the ratio between the linear moment and the nonlinear moment of the wall at the base ($R_{eq} = M_L/M_{NL}$). The factor is set at the wall base, where yielding was observed on walls. Nonlinearity is based on flexural behavior in the model, which is consistent with design codes (e.g., [2,3,6,22]) that promote flexural failure over shear failure. The level of nonlinearity is represented by R_{eq}, where the larger the value, the further the linear moment (M_L) separates from the nonlinear moment (M_{NL}). The dynamic shear amplification factor (ω_{v*}) represents the ratio between the shear from the nonlinear analysis (V_{NL}), and the shear from a linear analysis (V_L), which is reduced by the equivalent response modification factor. That is, it corresponds to the ratio between the shear in the nonlinear response and the shear from the equivalent linear analysis. According to the formulation, it is equivalent to the ratio between the base moment over the base shear for the linear behavior divided by the same expression, but for the nonlinear response. Recalling that the moment to shear ratio corresponds to the location of the equivalent lateral force, $\frac{M_L}{V_L}/\frac{M_{NL}}{V_{NL}}$ represents the change (ratio) in the equivalent lateral load location between the linear and nonlinear response. Thus, we have,

$$\omega_V^* = \frac{V_{NL}}{\frac{V_L}{R_{eq}}} = \frac{M_L}{V_L}/\frac{M_{NL}}{V_{NL}} \tag{2}$$

For the calculation of the dynamic shear amplification factor, a subset of data over the time series is selected where the bending moment for the nonlinear analysis falls between $0.72M_{NL,\,max}$ and $M_{NL,max}$, where $M_{NL,max}$ represents the maximum moment achieved by each wall in the nonlinear time history analysis (NLTHA). The 72% was selected to account for a 40% of moment overstrength [23] (~1/1.4) compared to the maximum reached value. The overstrength considers the probable moment ($M_{pr} = 1.25M_n$) and the moment strength reduction factor ($\phi = 0.9$), yielding a value of 1.4 (~1.25/0.9). The idea of establishing this criterion is to have consistency with the spectral modal analysis, which considers an envelope, while in the time-history analysis the maximum shear and moment do not occur at the same instant; although, the maximum shear associated with the maximum amplification occurs near the maximum bending moment.

In Fig. 10, the diagrams of shear, moment and deformed shape for the instance of maximum shear amplification are shown schematically for a coupled wall case. The results of the linear time-history and nonlinear time-history analyses are shown for comparison. Graphically, it is observed that the lineal model presents a deformed shape that resembles the first mode of vibration (Fig. 10a), whereas in the nonlinear model once the plastification of the base occurs, the deformed shape resembles the second natural mode of vibration (Fig. 10b). The shear amplification factor can be interpreted as the reduction of the height of the resultant of the inertial forces on the wall M1 and M2, when comparing the linear (M_L/V_L) and nonlinear (M_{NL}/V_{NL}) cases, as depicted in Fig. 10 and described in Eq. (2). For the example in Fig. 10, the resultant of the inertial forces reduces from $0.31h_w$ and $0.1h_w$ to $0.13h_w$ and $0.05h_w$ for M1 and M2, respectively.

3.1. Frequency ratio and system resonance

It is important to understand how the natural frequencies of the models (f_e) interact with the frequency content of the earthquake

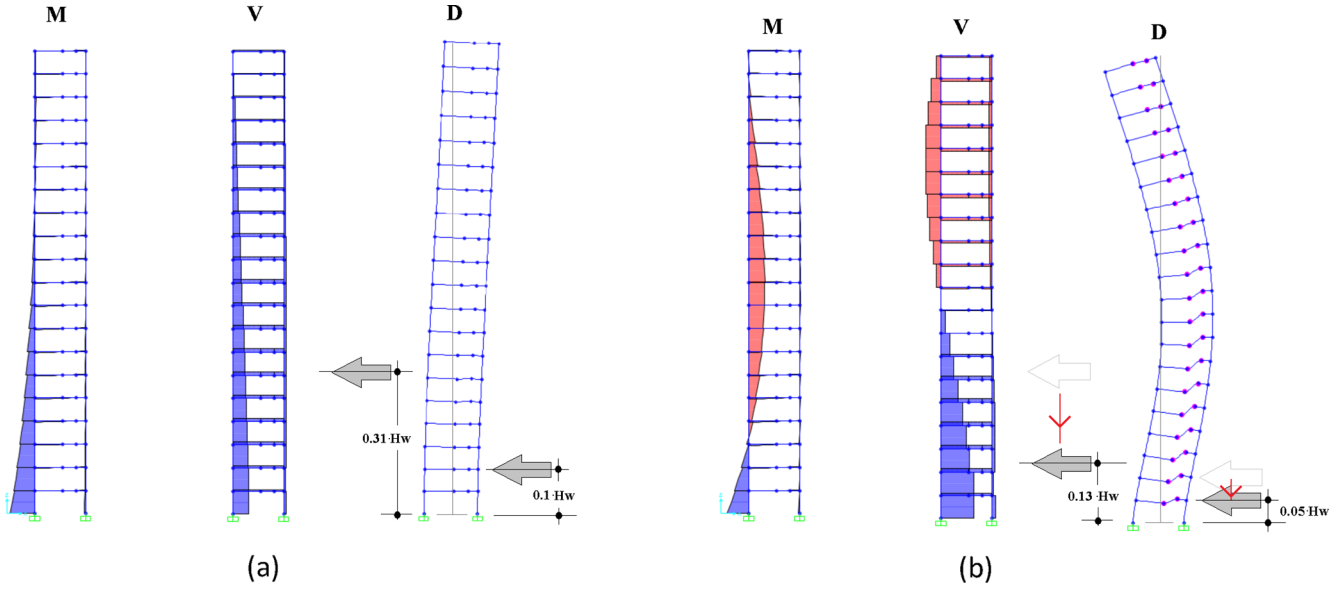

Fig. 10. Resultant of lateral inertial force for coupled walls for – (a) linear analysis, and for (b) nonlinear analysis.

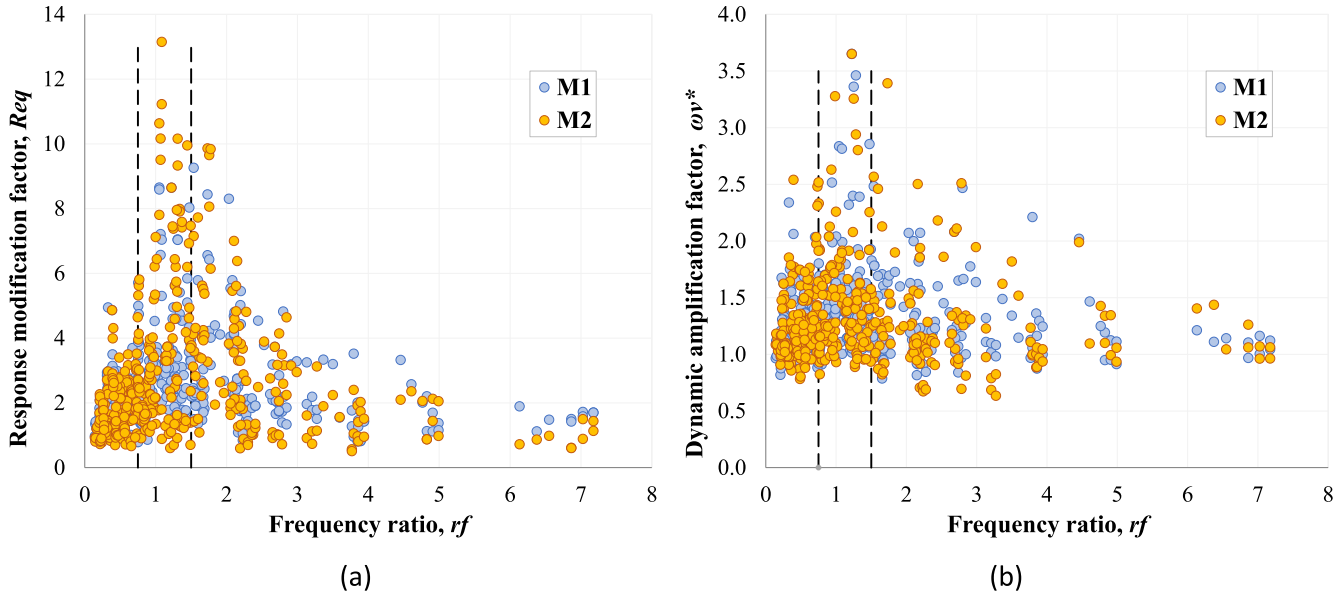

Fig. 11. (a) Frequency ratio (Rf) versus equivalent response modification factor (R_{eq}), and (b) Frequency ratio (Rf) versus dynamic shear amplification factor (ω_v*).

records or the average frequency of the records (f_m) since resonance increases the nonlinear incursion of the walls. Strictly speaking, the word resonance should be used for linear systems or the linear response; however, it is used here to recognize the frequency range with an amplified response. The frequency of the models (f_e) is defined as $f_e = \sum_{i=1}^{n} f_i \cdot f_{pmi}$, where f_i is the frequency of mode i, f_{pmi} is the modal participation factor of mode i and n is selected as the number of modes that accumulate 90% of the mass system (a larger accumulation of mass system did not change f_e considerably). Thus, the frequency ratio ($r_f = \frac{f_e}{f_m}$) is a good estimator to visualize its impact in the nonlinear response (R_{eq}) and dynamic shear amplification (ω_v*). Fig. 11b shows the behavior of the frequency ratio versus the dynamic shear amplification factor for all cases (each point represents an analysis distinguishing both coupled walls, M1 and M2). It can be noted that there is a concentration of high values for ω_v* between approximately $r_f = 0.75$ and $r_f = 1.5$, with several values of ω_v* over 2.5, which means that in general, resonance results in larger amplification. Fig. 11a shows how the frequency ratio is related to the equivalent response modification factor, with similar results as for the dynamic shear amplification factor, although values over 6 are also observed for frequency ratio close to 2.0.

Considering that resonance is observed for r_f values between approximately 0.75 and 1.5, the relation between the amplification factor (ω_v*) and the equivalent response modification factor (R_{eq}) is shown in Fig. 12, distinguishing between resonant (r_f = 0.75–1.5) and nonresonant cases. Fig. 12a shows the results for the resonant cases, yielding high values of both factors, with a maximum amplification value of ω_v* = 3.7 for R_{eq} = 8.7, and a maximum response modification factor of R_{eq} = 13.2. Fig. 12b shows the results for nonresonant cases with smaller values of ω_v* and R_{eq} compared to the resonant case, but with a similar trend between ω_v* and R_{eq} (trend lines are shown for walls M1 and M2 in Fig. 12). The maximum amplification value observed for nonresonant cases is ω_v*~2.5, that is, showing a reduction of 30% of the maximum amplification value of the resonant cases. On the other hand, the maximum value of the equivalent response modification factor also decreases considerably (from 13.2 to 8.3).

3.2. Effect of axial load

Fig. 13 shows ω_v* versus R_{eq}, where the equivalent response modification factor is multiplied by the wall top displacement sign for the instant of maximum amplification. This multiplication helps observing the impact of the direction in the response of the wall (ω_v* and R_{eq}), given that the axial load due to coupling would be reducing or increasing the total axial load on the walls depending on the loading direction. In the case of the wall M1 (longer wall), larger R_{eq} values are observed in the positive direction, with similar amplification values. The largest R_{eq} value for M1 is 9.3 in the positive direction, whereas the value is 5.8 in the negative direction. In the case of M2 (smaller wall), the differences are smaller between both directions.

An important impact of coupling is the variation in the axial load that exists on the vertical elements with the presence of seismic actions. During the lateral displacements imposed by the earthquake, the axial load will fluctuate increasing or decreasing its value from the static gravity load, where in general the lower the axial load, the lower the value of M_{NL}, which translates into a greater value of R_{eq} with a smaller value of V_{NL}. In Fig. 14a, the comparison between the amplification factor (ω_v*) with respect to R_{eq} (including the displacement sign) is plotted for wall M1. Similarly, Fig. 14c shows the level of axial load ($P/A_g f'_c$) with respect to R_{eq} also for M1, allowing understanding the effect of the axial load when compared to Fig. 14a. The blue lines in the figure indicate the levels of axial load due to gravitational actions. The positive direction for M1 commonly shows a reduction of axial load in the coupled wall. The reduction of axial load usually causes a decrease in moment strength (associated to M_{NL}) as commonly seen in P-M interaction diagrams (for moderate axial load), such that R_{eq} (M_L/M_{NL}) increases given a smaller nonlinear base moment (M_{NL}). In general, a larger coupling implies a larger variation of axial load, although some cases present a larger variation of axial loads for the coupling case with 0.3% of steel ratio in the slab (ρs = 0.3%).

The maximum axial load reaches values of $0.24A_g f'_c$ for the negative direction, which is about twice the gravitational axial load. The average axial load level in the negative direction in Fig. 14c increases from $0.1A_g f'_c$ to about $0.13A_g f'_c$ for ρs = 0.3% and ρs = 0.6%. In the case of the positive direction, most cases present a reduction in the axial load, reaching even negative axial load values that imply tensile forces. The impact of tensile forces is associated with a reduction in the wall flexural strength (compared to zero axial load). The average axial load level in the positive direction in Fig. 14c decreases from $0.1A_g f'_c$ to $0.07A_g f'_c$ and $0.04A_g f'_c$ for ρs = 0.3% and ρs = 0.6%, respectively. Even though there is a variation in the axial load due to the loading direction (Fig. 14c), the general trend between ω_v* and R_{eq} (Fig. 14a) is maintained (trend lines are solid lines with consistent color for the different coupling cases), yielding similar representative trend lines for both

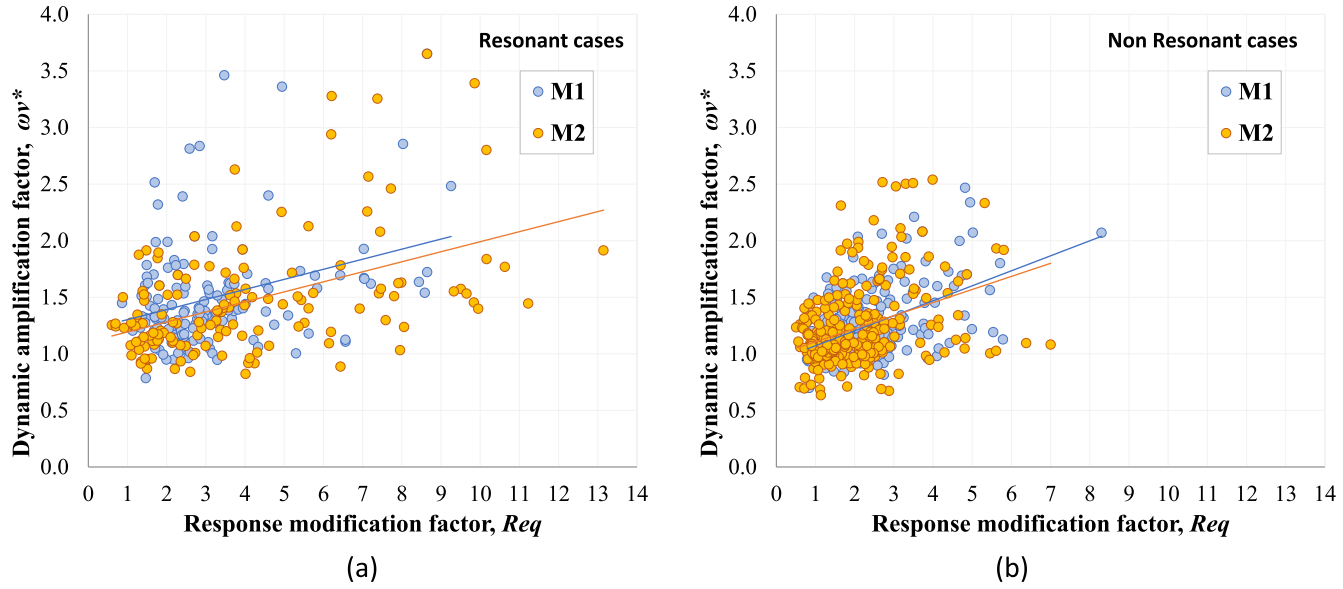

Fig. 12. – Equivalent response modification factor (R_{eq}) versus dynamic shear amplification factor (ω_v*) - (a) resonant cases, and (b) nonresonant cases.

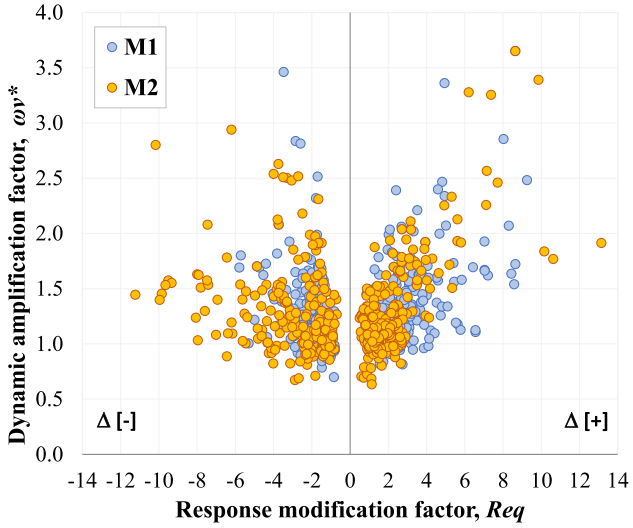

Fig. 13. - Equivalent response modification factor (R_{eq}) versus dynamic shear amplification factor (ω_v*) with respect to the displacement direction.

loading directions. However, the trend lines are different for different coupling levels. The results for the smaller wall M2 (Fig. 14b,d) are similar to M1, but variation in axial load is larger in some cases given the smaller size of the wall.

3.3. Shear

It is important to mention that the maximum base shear experienced by the walls in the analysis does not necessarily coincide with the shear reached at the maximum dynamic shear amplification value. Fig. 15a shows the shear force in the wall M1 for the maximum amplification normalized by the maximum shear of the NLTH analysis (r_{cm}). It can be seen that there are many values near 1. The average value of the shear ratio is 92% for positive and negative displacement, which indicates that, although the shear of the maximum amplification and the maximum shear are not coincident, they are close. The results for wall M2 are shown in Fig. 15b with similar results as for M1 in terms of range and average values, although smaller values are presented in the negative direction. The average values between the shear at maximum amplification and maximum shear are 90% and 87%, for positive and negative displacement, respectively.

Another relevant aspect of the shear magnitude (V_{NL}) is its comparison with the wall concrete shear strength (V_c) or maximum shear strength. The concrete shear stress strength of a wall is given by the ACI318-19 equation [3], as $v_c = 0.17\sqrt{f_c'}$ (f_c' in MPa). The maximum shear stress strength is then determined as $v_{n,max} = 0.83\sqrt{f_c'}$ (f_c' in MPa) ($v_{n,max} \sim 5v_c$) [3]. Fig. 16a shows, for the wall M1, the normalized shear force with respect to the concrete shear strength (V_1/V_c). For coupled and connected cases, the shear force reaches values close to 2.5 times the shear strength of concrete (V_c) for both directions. The average shear force normalized by the concrete shear strength for the wall M1 with a coupling of 0.3% is 1.09 and for a coupling of 0.6% is 1.2. Similar to Fig. 16a, Fig. 16b shows the normalized shear force, but for the wall M2. It can be observed that when the displacement is negative, the shear forces are low and barely exceed the shear strength of concrete. For positive displacement, the shear forces exceed the concrete shear strength for coupled cases. The average shear force over the concrete shear strength value in the wall M2 for a coupling of 0.3% is 0.61 and for a coupling of 0.6% is 0.66. These results reveal the important migration of shear forces to the longer wall M1 and the little impact on the shear design of the smaller wall M2.

4. Shear amplification of coupled walls

To observe the dependency of the different model variables to the dynamic shear amplification (ω_v*), regression (trend) lines are constructed versus the equivalent response modification factor (R_{eq}). Fig. 17a shows the regression models for the three cases that involve variations in wall height (10, 20 and 30 floors). It can be seen that there are modest differences in the amplification factors between the three cases. The largest slope of the trend lines corresponds to the 20-story models, because many resonant responses are given for a range of fundamental periods between 1 s and 2.5 s (~70% of the 20-story buildings). In the case of 30-story buildings, the low slope/dependency is related to the little nonlinear incursion of most models given the tall wall height that results in large yield lateral displacement, and the frequency content of the selected records that generate modest displacement demands in tall buildings (large period structures). Fig. 17b shows the amplification expressions for the M1 and M2 walls, and as can be seen both expressions are similar with a slightly larger slope for M1 given that coupling has a smaller impact in wall M1 compared to wall M2. The regression models in Fig. 17c show that resonant and

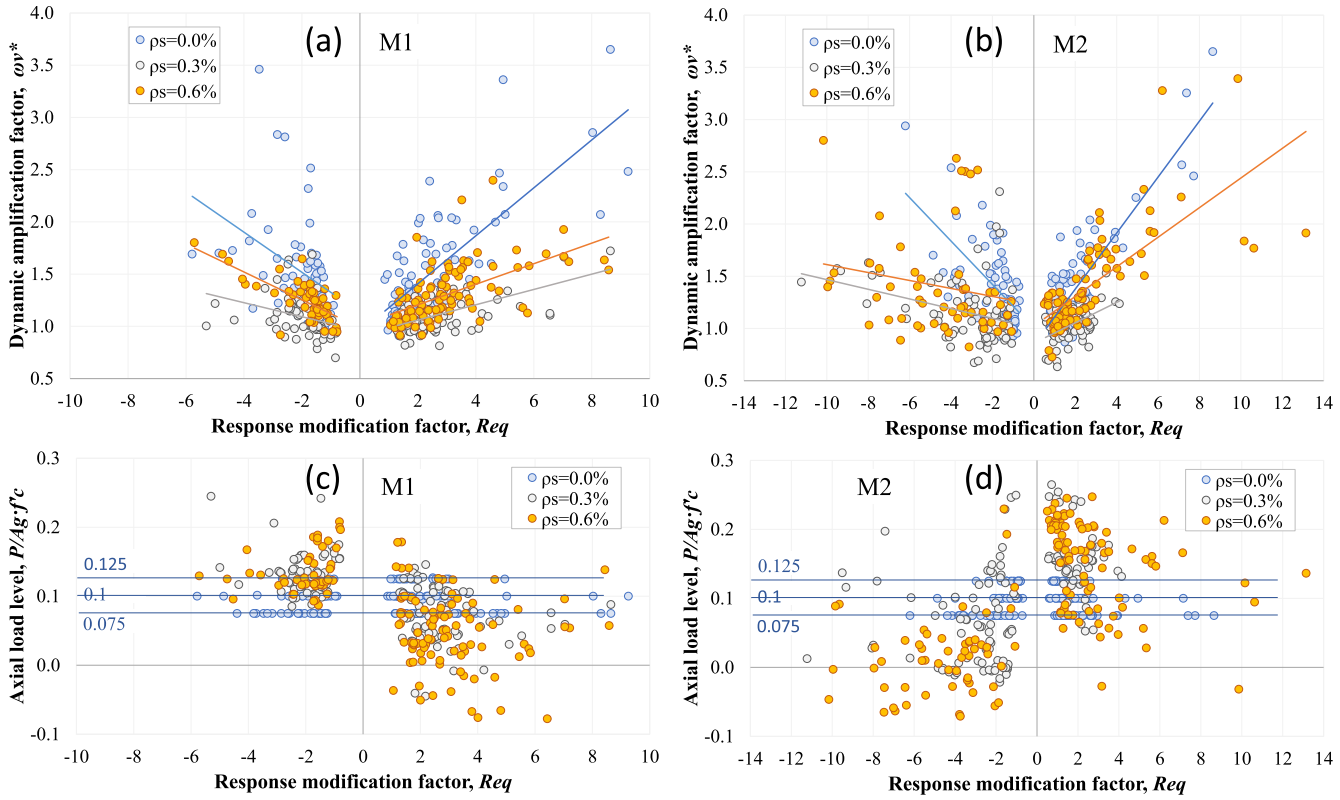

Fig. 14. (a, b) Dynamic shear amplification factor (ω_v*) and (c, d) axial load level (P/f'_cA_g) for (a, c) wall M1 (longer) and (b, d) wall M2 (smaller).

nonresonant cases behave similarly in terms of trend, noting that the resonant values present the largest values of shear amplification and equivalent response modification factors. That is, although for non-resonant cases most ω_v* and R_{eq} values are smaller than in resonant cases, they present similar dependency.

As was mentioned before, the dependency of the coupling effect is relevant given the axial load fluctuation in walls that yields moment strength variation. In the case of large values of R_{eq} (M_L/M_{NL}), generally associated with a reduction of axial load that decreases the moment strength (related to M_{NL}), the nonlinear shear force (V_{NL}) migrates to the more compressed element. That compensates the effect of large R_{eq} values, presenting moderate values of shear amplification $\omega_V^* = V_{NL}/\frac{V_L}{R_{eq}}$.

A modest amount of coupling would reduce the shear amplification factor. However, high levels of coupling can increase the shear amplification close to the response of connected walls since the structural system would become a cantilever wall with a combined section constituted by both walls. Thus, the data is reviewed for the different levels of coupling (Fig. 18). A regression equation is shown for the average shear amplification estimation. Although there is a large scatter for all coupling levels, there is a clear difference in shear amplification

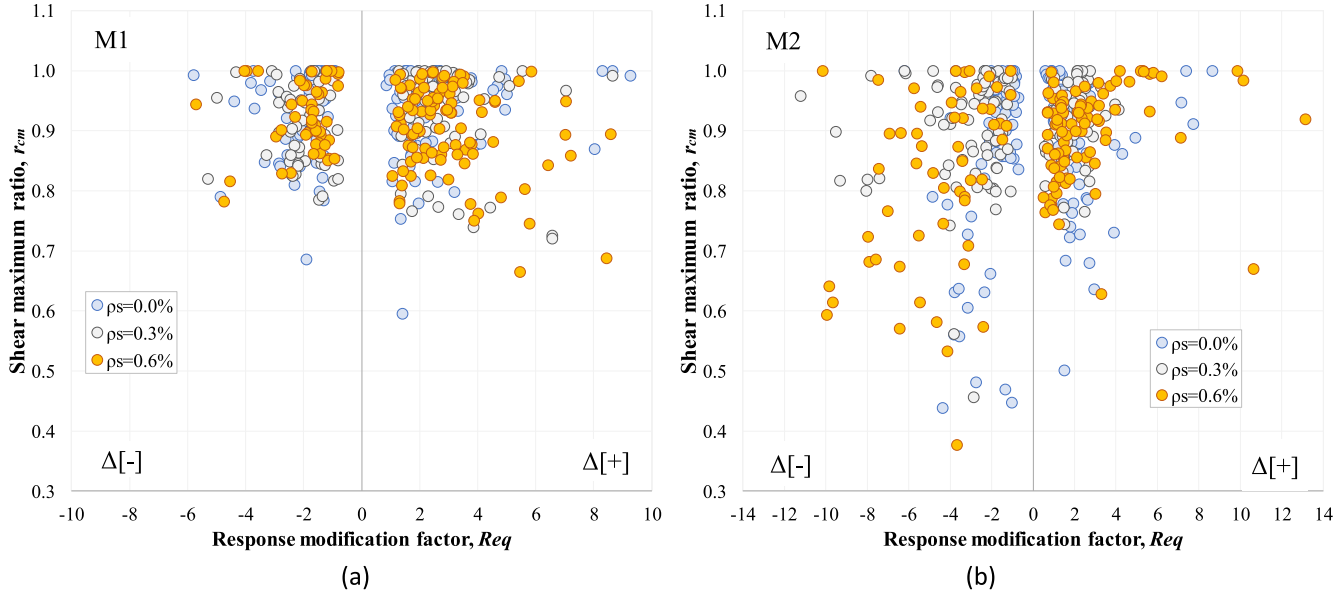

Fig. 15. Ratio of shear force for maximum amplification over maximum shear of the NLTH analysis – (a) M1, and (b) M2.

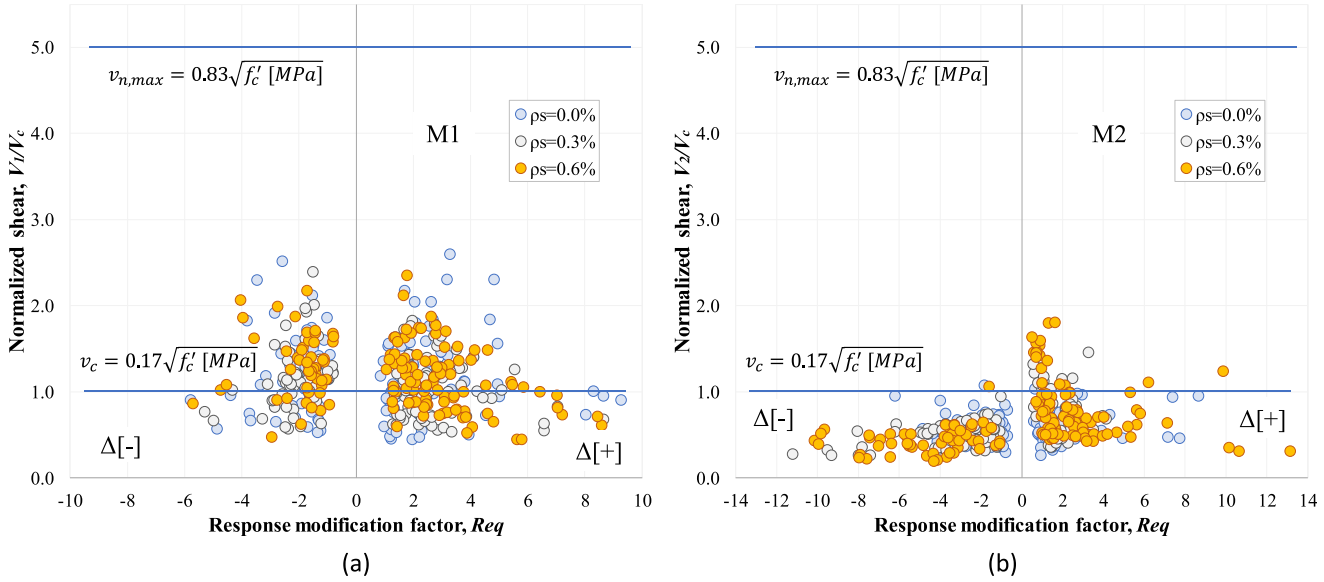

Fig. 16. Ratio of shear force over shear concrete strength (V_c) – (a) M1, and (b) M2.

between the different coupling cases, especially coupled (Fig. 18b,c) versus uncoupled (Fig. 18a - connected walls) cases, with larger amplification for the connected walls. The average expression for cases without coupling (ρs = 0.0% - connected walls) is,

$$\omega_v^* = 0.96 + 0.23R_{eq} \quad (3)$$

Fig. 18a shows the linear regression model constructed to explain the dynamic shear amplification dependency to the equivalent response modification factor. The mean amplification of the data is $\omega_v^* = 1.45$. If the average regression line is analyzed (Eq. (3)), it can be noted that for values of $R_{eq} = 1$, the mean amplification value is $\omega_v^* = 1.19$, which suggests that in general the amplification always exists in reinforced concrete structures caused by the change in stiffness due to cracking. Even for $R_{eq} < 1$, it can be seen values with $\omega_v^* > 1$. This is triggered by the shear force increase in the nonlinear model under moderate seismic actions that cause wall cracking, but without yielding, which deviates from the linear model that uses gross section. The average expression for the coupling cases with steel amount of ρs = 0.3% is,

$$\omega_v^* = 0.95 + 0.06R_{eq} \quad (4)$$

Fig. 18b shows the behavior of the shear dynamic amplification factor for models with ρs = 0.3%. The mean amplification of the data is $\omega_v^* = 1.1$, thus moderate amplification levels are observed given the axial load fluctuation and moment redistribution due to coupling, showing a change rate between ω_v^* and R_{eq} of 0.06 (1/4 of the slope observed in the connected cases). The average expression for the coupling cases with steel amount of ρs = 0.6% is,

$$\omega_v^* = 1.06 + 0.09R_{eq} \quad (5)$$

Fig. 18c shows the behavior of the shear dynamic amplification factor for models with ρs = 0.6%. The mean amplification of the data is $\omega_v^* = 1.35$, thus higher amplification levels are observed compared with the case of ρs = 0.3%, but still lower compared to the connected wall cases. This result indicates that the higher level of coupling is making the overall system resemble the response of connected walls, but as a system with two walls. The values obtained for moderate coupling (ρs = 0.3%, 0.6%) are considerably smaller than the values observed

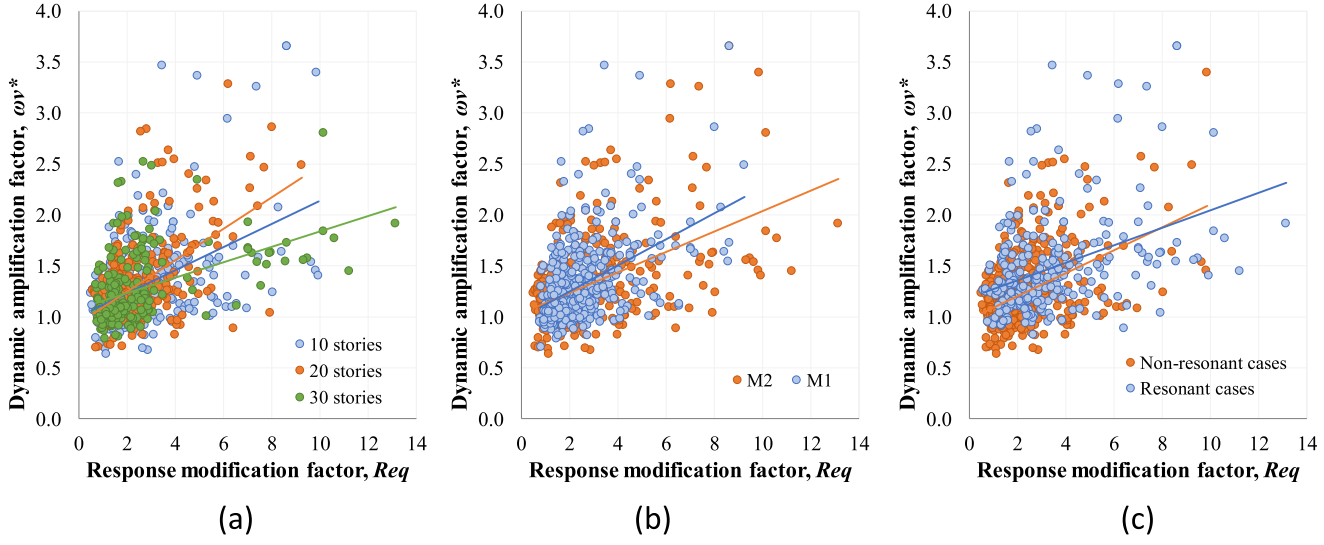

Fig. 17. Correlation between dynamic shear amplification factor (ω_v*) and equivalent response modification factor (R_{eq}) – (a) number of floors, (b) wall length, and (c) resonance.

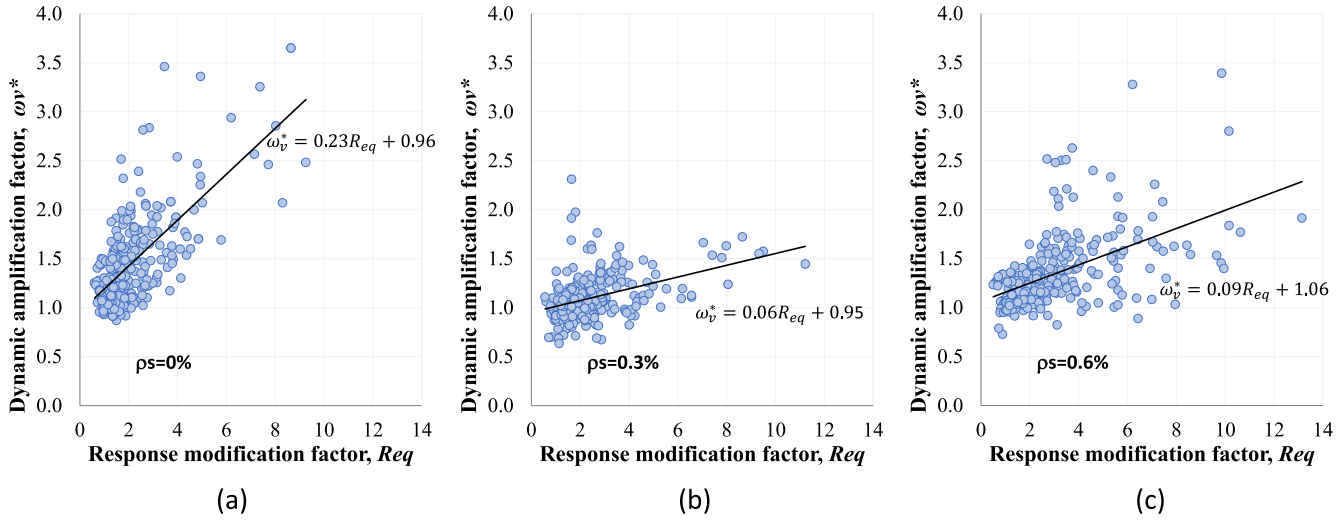

Fig. 18. Correlation between dynamic shear amplification factor (ω_v*) and equivalent response modification factor (R_{eq}) for – (a) connected walls, (b) coupling with ρs = 0.3%, and (c) coupling with ρs = 0.6%.

for connected walls (Fig. 18b, c versus Fig. 18a). This indicates that cantilever walls are more prone to present dynamic shear amplification than coupled walls, as long as the coupling is not big enough to make the system to behave as a unit with two walls.

The level of coupling was calculated based on the maximum wall moment (gravitational load) and the maximum moment in coupling elements. The coupling level (Tl/M_b, where Tl is the moment generated by the variation of axial load in walls due to coupling and M_b is the overall base moment) was estimated on average as 0.22 for ρs = 0.3% and 0.34 for ρs = 0.6%. Most analyses and tests in the literature have tried values between 0.35 and 0.8 [24], and Harris [25] proposed a practical limit of 0.66. This last limit differentiates between partially and fully coupled walls [25]. Thus, the values observed in this work can be considered moderate.

As shown previously, the shear amplification factor depends on two main parameters: the coupling level and the equivalent response modification factor. However, many design codes and earlier investigations based on cantilever walls relate the shear amplification mainly to the number of stories, which as shown here, such dependency is modest and even reduce with tall buildings (e.g., 30 stories) when we consider moderate coupling, given the large elastic displacement that needs to be overcome to present incursions into the nonlinear response. Other records with larger amplitude in the frequency content closer to the period of tall buildings might increase the shear amplification due to larger nonlinear incursions. Thus, the equations for ρs = 0.3% and ρs = 0.6% (Eqs. (4) and (5)) for shear amplification are used to derive expressions based on the Chilean code, allowing a direct comparison with the expression in ACI 318–19 (similar to other design codes). Since the ACI 318 equation is related to the number of stories, it is necessary to establish a relationship between the equivalent response modification factor (R_{eq}) and the number of stories.

The expression for R_{eq} is established based on the code requirements for the Chilean earthquake-resistant design (D.S. 61 [22]), with an overstrength factor of Ω = 1.4 [23], as the ratio between the linear shear force (V_L) and the shear design force. The shear design force ($\frac{V_L}{R^*}$) is defined as the linear shear force reduced by the modal response modification factor $R^*(T) = 1 + \frac{T}{0.1 \cdot T_o + \frac{T}{11}}$, with a minimum shear force of V_{min}. Eq. (6) shows the behavior of the equivalent response modification factor according to the seismic design code, D.S. 61 [22]. Thus, R_{eq} is established as,

$$R_{eq} = \frac{V_L}{1.4 \cdot max\left(\frac{V_L}{R^*}, V_{min}\right)} = \frac{S_o(T)}{1.4 \cdot max\left(\frac{S_o(T)}{R^*(T)}, \frac{1}{6}\right)} \quad (6)$$

where, $S_o(T) = \frac{1 + 4.5 \cdot \left(\frac{T}{T_o}\right)^p}{1 + \left(\frac{T}{T_o}\right)^3}$ is the amplification factor of maximum effective acceleration, T_o and p are soil parameters, and T is the period of the structure.

From the development of Eq. (6), it can be seen that the behavior of R_{eq} depends exclusively on the fundamental period (T) and the soil parameters T_o and p (T_o = 0.3 and p = 1.5 for soil type B; T_o = 0.75 and p = 1 for soil type D). To establish the period of the structure, the stiffness index obtained from Guendelman et al. [14] is used for buildings of normal stiffness in Chile, which correspond to values ranging from H/T = 40 m/s to H/T = 70 m/s. The height of the building (H) is calculated considering a story height of 2.5 m, and cracking is introduced with a multiplier of 1.5 for the period [22]. Given that the expressions for shear amplification (Eqs. (4), 5) depend on R_{eq}, Eq. (6) helps to relate it to the number of floors (ns) by setting the value of H/T to either 40 m/s or 70 m/s, where $H = 2.5m \bullet ns$. Fig. 19 shows the behavior of the dynamic shear amplification factor for soil types B ($v_{s30} \geq$ 500 m/s) and D ($v_{s30} \geq$ 180 m/s). The shown lines correspond to stiffness indices of H/T = 40 m/s (orange) and H/T = 70 m/s (green) using the proposed expressions for shear amplification for ρs = 0.3% and ρs = 0.6% (Eqs. (4) and (5)). The values determined for R_{eq} are relatively low (indicating low nonlinear incursion), ranging between 1 and 5 for most cases, as same as observed by others for Chilean buildings (e.g., [23]). Fig. 19 also includes the expression used in ACI318-19, which corresponds to Eq. (1) increasing the shear amplification with the number of floors and with a cap of 1.8 that coincides with 15 floors. For soil type B (Fig. 19a), it can be seen that the amplification factor of ACI318-19 largely overestimates the amplification for ρs = 0.3%. Similar results are obtained for ρs = 0.6%, but in this case, the differences are smaller for shorter buildings, whereas for taller buildings (over 15 stories) the minimum shear design force of D.S. 61 yields much smaller shear amplification factors than ACI 318–19, given the small R_{eq} values. Fig. 19b shows the behavior of the amplification factor for type D soil. It can be seen that when using the design parameters of D.S. 61 and the proposed shear amplification for ρs = 0.3% and ρs = 0.6%, the amplification factor of the ACI318-19 still presents larger values given the moderate coupling of walls and small values of R_{eq}. Such a trend might be reverted when using the expression for cantilever walls (Fig. 18a) instead of the expressions for coupled walls (Fig. 18b,c), resulting in even larger shear amplification values compared with ACI 318–19. The results of Fig. 19 are valid for coupled walls with moderate coupling levels, as it is commonly seen in walls coupled with slabs.

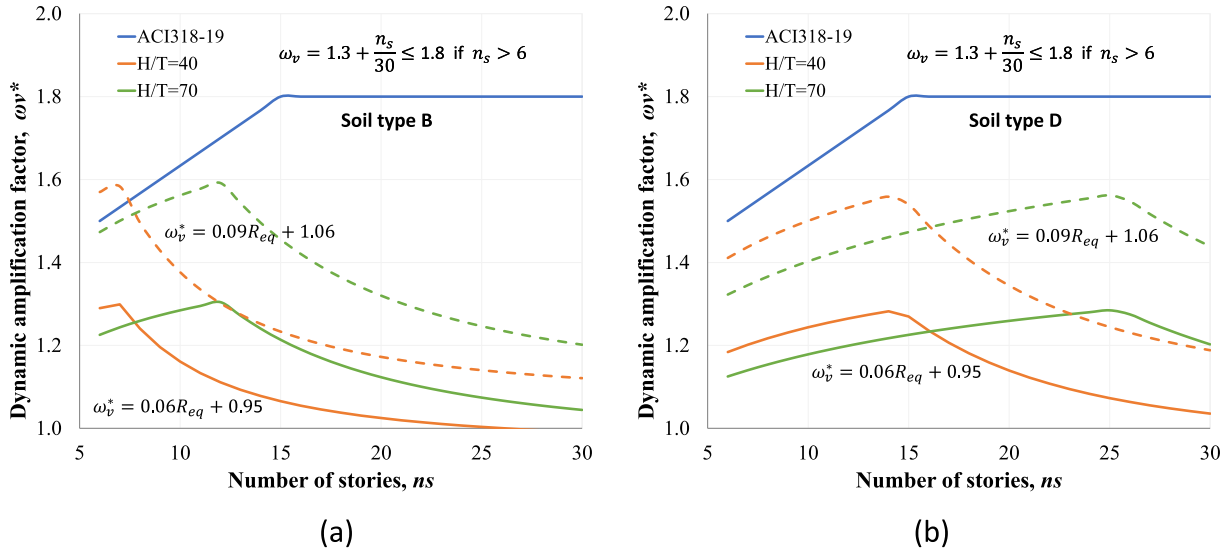

Fig. 19. Comparison between the proposed dynamic shear amplification factor (ω_v*) consistent with D.S. 61 [22] and ACI 318–19 [3] for – (a) soil type B, and (b) soil type D.

5. Conclusions

In this work, a parametric study is carried out that covers 432 nonlinear time-history analyses (including 6 records) for two coupled walls of different length (one has a fixed length of 2 m), including variations in the amount of steel ratio of the boundary element (1%, 3% and 5%), amount of steel ratio in the coupling element (0.0%, 0.3% and 0.6%), building number of stories (10, 20 and 30) and wall length (2 m, 4 m and 6 m) to capture the dynamic shear amplification. The formulation considers nonlinearity of walls with fiber models, while the coupling beams/slabs are elastic with rigid-perfectly plastic hinges at element ends.

There is a correlation between the dynamic shear amplification factor (ω_v*) and the equivalent response modification factor (R_{eq}). The dynamic shear amplification factors of connected wall systems are larger than those presented in coupled walls (Fig. 18). The mean amplification value for connected walls is $\omega_v^* = 1.45$, whereas for the coupled cases the mean values are $\omega_v^* = 1.1$ for $\rho s = 0.3\%$ and $\omega_v^* = 1.35$ for $\rho s = 0.6\%$. The high amplification values in connected walls are caused by the concentration of the nonlinearity sources of the system at the base of the walls, and therefore, once yielding occurs, a marked influence of the upper modes begins. In addition, the connected cases do not show fluctuations in the axial load in the walls, which implies that there are no variations of the moment strength and therefore the shear associated with it. In the case of coupled walls, the variation of the axial load caused by the coupling slabs reduces the moment strength of the unloaded wall and increases the moment strength in the more compressed wall, generating in cases that have high amounts of steel in the coupling elements tensile axial loads in the unloaded wall (Fig. 14).

The cases with coupling elements with $\rho s = 0.3\%$ yield low levels of shear amplification, whereas for the cases with coupling elements with $\rho s = 0.6\%$, they present closer results to connected walls, since the overall system leans towards a response as a cantilever wall with a combined section of two walls. The results for the wall M2 (smaller) indicate that the amplification for this element is practically irrelevant since, for the presented cases, the shear concrete strength is sufficient to withstand the shear actions (Fig. 16).

The expression of the ACI318-19 based on cantilever walls, as same as with other design codes, relates the dynamic shear amplification factor with the number of stories, but in general, it does not correlate well with coupled tall walls that present moderate nonlinear incursions or buildings designed with a minimum base shear, which results in low R_{eq} values. In general, the ACI 318–19 expression overestimates the dynamic shear amplification factor, in particular in walls with moderate coupling, which in this case corresponds to average coupling levels of 0.22 for $\rho s = 0.3\%$ and 0.34 for $\rho s = 0.6\%$ (Fig. 19). Such differences would not be observed if connected walls were compared with ACI 318-19.

Declaration of Competing Interest

The authors declare that they have no known competing financial interests or personal relationships that could have appeared to influence the work reported in this paper.

Appendix A. Supplementary material

Supplementary data to this article can be found online at https://doi.org/10.1016/j.engstruct.2020.110867.

References

[1] Blakeley R, Cooney R, Megget L. Seismic Hear Loading at Flexural Capacity in Cantilever Wall Structures. Bulletin New Zealand National Soc Earthquake Eng 1975;8(4):278–90.
[2] NZS 3101: Part1, Concrete Structures Standard; Part2, Commentary on the design of concrete structures 2006. Wellington, New Zealand.
[3] Building Code Requirements for Structural Concrete (ACI318-19) and Commentary. American Concrete Institute. Farmington Hills, Michigan, USA, 2019.
[4] Derecho AT, Iqbal M, Fintel M, Corley WG. Loading History for Use in Quasi-static Simulated Loading Test. Reinforced Concrete Structures Subjected to Wind and Earthquake Forces, ACI Special Publication SP-63 1980: 329–344.
[5] Eibl J, Keinzel E. Seismic shear forces in RC cantilever shear walls, 9th World Conference on Earthquake Engineering, 1988, Japan.
[6] EN 1998-1: 2004. Eurocode 8: Design of structures for earthquake resistance – Part 1: General rules, seismic actions and rules for buildings, 2004.
[7] Does Priestley M. Capacity Design Do the Job? An Examination of Higher Mode Effects in Cantilever Walls. Bull. of the. New Zealand Society for Earthq. Eng. 2003;36(4):276–92.
[8] Panagiotou M, Restrepo JI. Lessons learnt from the UCSD full-scale shake table testing on a 7-story residential building. Squaw Creek: SEAOC Convention; 2007.
[9] Eberhard MO, Sozen MA. Behavior-Based Method to Determine Design Shear in Earthquake-Resistant Walls. J Struct Eng 1993;119(2):619–40.
[10] Vuran E. Shear migration and dynamic shear amplification effects on seismic response of core walls. Bull Earthq Eng 2018;16(10):5003–15.
[11] Spacone E, Filippou FC, Taucer FF. Fibre beam-column model for non-linear analysis of RC frames: Part 1 Formulation. Earthquake Eng Struct Dynamics 1996;25:711–25.
[12] Clough RW, Benuska KL, Wilson EL. Inelastic earthquake response of tall buildings. 3rd World Conference on Earthquake Engineering New Zealand. 1965.

[13] Estay C. Characteristics of reinforced concrete wall design in Chile (in Spanish). Civil Engineering Thesis 2008. School of Engineering. University of Chile.
[14] Guendelman T, Guendelman M, Lindenberg J. Bio-Seismic profile of buildings (in Spanish). VII Conference of Seismology and Seismic Engineering and First Ibero-American Congress of Seismic Engineering, 1997, La Serena, Chile.
[15] Saatcioglu M, Razvi S. Confinement Model for High-Strength Concrete. J Struct Eng 1999;125(3):281–9.
[16] Welt TS, Massone LM, LaFave JM, Lehman DE, McCabe SL, Polanco P. Confinement Behavior of Rectangular Reinforced Concrete Prisms Simulating Wall Boundary Elements. Journal of Structural Engineering-ASCE 2017;143(4):04016204https://doi.org/10.1061/(ASCE)ST.1943-541X.0001682.
[17] SAP2000® version 21. Computers & Structures, INC (2018). CSI Analysis Reference Manual. Walnut Creek, California, USA.
[18] Rathje EM, Abrahamson NA, Bray JB. Simplified frequency content estimates of earthquake ground motions. J Geotech Geoenviron Eng 1998;124(2):150–9.
[19] Jiménez FJ, Massone LM. Experimental seismic shear force amplification in scaled RC cantilever shear walls with base irregularities. Bull Earthq Eng 2018;16(10):4735–60.
[20] Massone LM, Díaz S, Manríquez I, Rojas F, Herrera R. Experimental Cyclic Response of RC Walls with Setback Discontinuities. Eng Struct 2019;178:410–22.
[21] Bass E. Dynamic shear amplification in reinforced concrete walls through time history nonlinear analysis (in Spanish). Master thesis in Structural, Earthquake and Geotechnical Engineering 2019, Universidad de Chile, Santiago, Chile.
[22] D.S. N 61 MINVU. Building seismic design code, replacing D.S N 117, 2010. Chilean Ministry of Housing and Urbanism, Diario Official; 13 December 2011 (in Spanish).
[23] Lagos R, Kupfer M, Lindenberg J, Bonelli P, Saragoni R, Guendelman T, et al. Seismic Performance of High-rise Concrete Buildings in Chile. Int J High-Rise Build 2012;1(3):181–94.
[24] El-Tawil S, Harries KA, Fortney PJ, Shahrooz BM, Kurama Y. Seismic Design of Hybrid Coupled Wall Systems: State of the Art. J Struct Eng 2010;136(7):755–69.
[25] Harries KA. Ductility and deformability of coupling beams in reinforced concrete coupled walls. Earthquake Spectra 2002;17(3):457–78.